JCTC Journal of Chemical Theory and Computation

A New Algorithm for Efficient Direct Dynamics Calculations of Large-Curvature Tunneling and Its Application to Radical Reactions with 9−15 Atoms

Antonio Fernández-Ramos

Departmento de Quimica Fisica, Facultade de Quimica, Universidade de Santiago de Compostela, 15782 Santiago de Compostela, Spain

Donald G. Truhlar*

Department of Chemistry and Supercomputing Institute, University of Minnesota, 207 Pleasant Street S. E., Minneapolis, Minnesota 55455-0431

Received June 15, 2005

Abstract: We present a new algorithm for carrying out large-curvature tunneling calculations that account for extreme corner-cutting tunneling in hydrogen atom, proton, and hydride transfer reactions. The algorithm is based on two-dimensional interpolation in a physically motived set of variables that span the space of tunneling paths and tunneling energies. With this new algorithm, we are able to carry out density functional theory direct dynamics calculations of the rate constants, including multidimensional tunneling, for a set of hydrogen atom transfer reactions involving 9−15 atoms and up to 7 nonhydrogenic atoms. The reactions considered involve the abstraction of a hydrogen atom from hydrocarbons by a trifluoromethyl radical, and in particular, we consider the reactions of CF_3 with CH_4, C_2H_6, and C_3H_8. We also calculate several kinetic isotope effects. The electronic structure is treated by the MPWB1K/6-31+G(d,p) method, which is validated by comparison to experimental results and to CBS-Q, MCG3, and G3SX(MP3) calculations for $CF_3 + CH_4$. Harmonic vibrational frequencies along the reaction path are calculated in curvilinear coordinates with scaled frequencies, and anharmonicity is included in the lowest-frequency torsion.

1. Introduction

Direct dynamics is "the calculation of rates or other dynamical observables directly from electronic structure information, without the intermediacy of fitting the electronic energies in the form of a potential energy function."[1] Although most direct dynamics calculations are based on classical mechanics for the nuclear motion,[2−6] there has also been progress in including quantized vibrations and tunneling.[1,7−12]

To make direct dynamics practical, one often uses inexpensive electronic structure methods, as in dynamics calculations based on semiempirical valence bond configuration interaction,[3] semiempirical molecular orbital theory,[1,2,8,9,12] or tight-binding molecular dynamics.[5] Using an affordable electronic structure method allows one to combine multidimensional tunneling calculations with variational transition-state theory (VTST/MT) for relatively large systems. Therefore, one can calculate thermal rate constants at a low computational cost without building an analytical potential energy surface. For example, one can use semiempirical molecular orbital theory with specific-reaction parameters (SRPs) fit to experimental or selected higher-level calculations.[1,9,12] This approach, although very successful in some cases, has the drawback that SRP surfaces do not form a model chemistry[13] and, hence, cannot be broadly validated. Another approach to lowering the cost is to use automatic and efficient fitting methods.[14] The third approach, which is

* Corresponding author. Phone: (612) 624-7555. Fax: (612) 624-9390. E-mail: editor@chem.umn.edu.

10.1021/ct050153i CCC: $30.25
Published on Web 08/25/2005

the one considered in the present article, is to improve the dynamical algorithms.

For reliable calculations of rate constants in reactions involving the transfer of a hydrogen atom, hydride ion, or proton, it is essential to include corner-cutting tunneling[7,9,15−19] in the calculation. The VTST/MT method is a well-validated[20,21] method for calculating reaction rate constants, including the contribution of corner-cutting tunneling, and when reaction-path curvature is small, it is very efficient because all required data can be obtained from a harmonic expansion of the potential around one[22,23] or more[12] minimum energy paths (MEPs). However, especially for bimolecular reactions involving the transfer of a light particle between two heavy atoms (the so-called heavy−light−heavy systems), additional information is required in the reaction swath (tunneling swath), which is defined[7,24] as the region on the concave side of the MEP where corner-cutting tunneling occurs. Large-curvature tunneling[9,17,19] (LCT) is tunneling that passes through the swath at a distance too far from the MEP to be uniquely or realistically represented by the aforementioned harmonic expansion. Proton, hydride, and hydrogen transfer reactions, especially those with symmetric or nearly symmetric barriers, often involve LCT in which the corner cutting is due to the reaction coordinate being strongly coupled to the hydrogen stretching vibration mode, resulting in a highly curved MEP. In fact, the most probable tunneling path is the best compromise between low-energy but long tunneling paths, near the MEP, and paths that are less favorable energetically but shorter, such as straight-line paths. The optimum path is the one with the least imaginary action.[18] It has been shown[20] that a good approximation to the tunneling probabilities calculated from the least-action path can be obtained by the microcanonical optimized multidimensional tunneling (μOMT) approximation,[9] in which tunneling probability, at each tunneling energy, is the maximum between the small-curvature tunneling (SCT) probability[8,25] evaluated with information obtained along the MEP and the LCT probability[9,17,19,25,26] evaluated with information from the reaction swath. One of the difficulties in evaluating the μOMT transmission coefficients by direct dynamics is the evaluation of the LCT probabilities, because, at least with current algorithms, they are very demanding in terms of the number of electronic structure calculations required for evaluations of the potential. In the present paper, we develop an approach based on a 2D-spline under tension that reduces the computer time by about 2 orders of magnitude without a loss of accuracy.

The gas-phase reactions in which the trifluoromethyl radical (CF_3) abstracts a hydrogen atom from hydrocarbons[27−32] are good examples of heavy−light−heavy systems with corner-cutting tunneling.[9] In this manuscript, we study the following reactions:

(A) CF_3 radical with methane:

$$CF_3 + CH_4 \rightarrow CF_3H + CH_3 \quad \text{(R1)}$$

$$CF_3 + HCD_3 \rightarrow CF_3H + CD_3 \quad \text{(R2)}$$

$$CF_3 + HCD_3 \rightarrow CF_3D + CD_2H \quad \text{(R3)}$$

$$CF_3 + CD_4 \rightarrow CF_3D + CD_3 \quad \text{(R4)}$$

Table 1. Vibrational-Frequency Scaling Factors and Energies (in kcal/mol Relative to Reactants) of Products and Saddle Point of Reaction R1

method	S	ΔE	ΔH_0	$V^{\ddagger}$	$\Delta V_a^{\ddagger}$
experiment		−0.7[a]	(−1.5)[b]		
G3SX(MP3)//MC-QCISD/3	0.9930	**−1.41**	**−2.42**	14.80	12.49
CBS-Q	0.9184[c]	**−0.91**	**−2.27**	**14.34**	**12.23**
MCG3/3//MC-QCISD/3	0.9930	**−1.53**	**−2.54**	14.69	12.38
MC3BB	0.9675[d]	0.84	−0.53	**15.09**	**12.68**
MC3MPW	0.9669[d]	−0.26	−1.46	**14.74**	**12.32**
MC-QCISD	0.9930	−1.33	−2.34	16.63	14.42
consensus[e]		−1.28	−2.41	14.72	12.41
MPWB1K/MG3S	0.9567[f]	0.84	−0.38	15.09	12.68
BB1K/MG3S	0.9590	1.00	−0.17	15.68	13.41
MPW1K/MG3S	0.9581	−0.01	−1.33	14.97	12.69
MPWB1K/DIDZ	0.9537	0.32	−0.85	14.39	12.06
BB1K/DIDZ	0.9561	0.51	−0.59	14.99	12.82
MPW1K/DIDZ	0.9515	−0.72	−1.83	14.42	12.23

[a] Liu et al.[23] [b] 298 K.[41] [c] HF/6-31G(d′).[33] [d] Zhao et al.[40] [e] Average of three bold entries. [f] Zhao and Truhlar.[39]

(B) CF_3 radical with ethane:

$$CF_3 + C_2H_6 \rightarrow CF_3H + C_2H_5 \quad \text{(R5)}$$

$$CF_3 + C_2D_6 \rightarrow CF_3D + C_2D_5 \quad \text{(R6)}$$

(C) CF_3 radical with propane:

$$CF_3 + C_3H_8 \rightarrow CF_3H + C_3H_7 \quad \text{(R7)}$$

$$CF_3 + C_3D_8 \rightarrow CF_3D + C_3D_7 \quad \text{(R8)}$$

We further subdivide R7 and R8 into R7p and R8p, in which a primary H or D is abstracted, and R7s and R8s, in which a secondary H or D is abstracted.

We first show that the new algorithm proposed to evaluate the LCT probabilities allows the evaluation of μOMT transmission coefficients for this kind of system with a reasonable computing time. Then we show that density functional theory (DFT) methods can be used for direct dynamics calculations of the thermal rate constants with optimized multidimensional tunneling even for reactions as complex as CF_3 with propane, which is a difficult case because it involves seven heavy (i.e., nonhydrogenic) atoms (the cost of the electronic structure calculations increases rapidly with the number of heavy atoms).

Section 2 presents the electronic structure calculations used to select a level of theory for the direct dynamics calculations. Section 3 presents the dynamical theory including the new 2D interpolation scheme. Section 4 gives details of the calculations. Section 5 gives results, and Section 6 gives a discussion.

2. Electronic Structure Calculations

The direct dynamics calculations in this paper are based on DFT because it provides a good compromise of affordability and accuracy. Several types of electronic structure calculations were performed for reaction R1 to find a reliable DFT method for the set of reactions R1, R5, and R7; all the methods employed are listed in Table 1. For bond energies, the most accurate methods employed here are CBS-Q,[33]

G3SX(MP3),[34] MC-QCISD/3,[35] and MCG3/3.[35] In tests against a data set of 109 atomization energies, these methods had mean unsigned errors per bond of 0.30, 0.22, 0.37, and 0.22 kcal/mol, respectively, and in a test against 44 barrier heights for H-atom transfer, they had mean unsigned errors of 0.87, 0.94, 1.33, and 1.01 kcal/mol, respectively.[36] In the present article, we employed MCG3/3 and G3SX(MP3) with geometrics and frequencies optimized at the MC-QCISD/3 level, whereas CBS-Q geometries were obtained as specified[33] by the developers of that method. In calculating zero-point energies in Table 1, all frequencies were scaled with empirical factors S, determined previously;[33,37−40] these factors are given in the table. (The use of the harmonic expressions with scaled frequencies may be called the quasiharmonic approximation.) For barrier heights, two more recently developed methods, MC3BB[40] and MC3MPW,[40] have even smaller mean unsigned errors, in particular, 0.78 and 0.75 kcal/mol, respectively. Therefore, G3SX(MP3), CBS-Q, and MCG3 are expected to be the most accurate of the methods employed here for reaction energies, and CBS-Q, MC3BB, and MC3MPW are expected to be the most accurate for barrier heights. We, therefore, used these methods to compute consensus best estimates for the following quantities: ΔE, classical energy of reaction; ΔH_0, zero-point-inclusive energy of reaction; $V^{\ddagger}$, classical barrier height; and $\Delta V_a^{G\ddagger}$, zero-point-inclusive barrier height evaluated at the saddle point. The last-named quantity is given in the harmonic or quasiharmonic approximation for bimolecular reactions by

$$\Delta V_a^{G\ddagger} = V^{\ddagger} + \frac{1}{2}\hbar \sum_{m=1}^{3N-7} [\omega_m(s=0) - \omega_m(s=-\infty)] \quad (1)$$

where $\hbar$ is Planck's constant divided by 2π, $\omega_m(s)$ is a generalized normal mode vibrational frequency in s^{-1} (that is, radians per second), and $\omega_m(s=0)$ and $\omega_m(s=-\infty)$ are the vibrational frequencies of mode m at the saddle point and the reactants, respectively. (For a unimolecular reaction, one would need to subtract $^1/_2\hbar\omega_{3N-6}(s=0)$ at the reactants, but this is zero for a bimolecular reaction. Note that when we quote numerical values of $\omega_m(s)$, we always give $\omega_m(s)/(2\pi c)$ in cm^{-1}, where c is the speed of light.) The consensus values of these four quantities are listed in Table 1, and they may be more accurate than the available experimental[41] values.

All of the levels discussed so far are more expensive than the DFT levels (given in the next sentence) that we considered for direct dynamics, and they only serve as benchmark calculations. The three DFT methods given in Table 1, namely, MPW1K,[37] BB1K,[38] and MPWB1K,[42] have previously been optimized for kinetics. In each, they have been applied with two basis sets: an augmented polarized triple-ζ basis set, MG3S,[43] and an augmented polarized double-ζ basis set, 6-31+G(d,p),[44] also called DIDZ. Table 1 indicates that the MPW1K/MG3S, MPWB1K/DIDZ, and MPW1K/DIDZ results are all reasonably accurate for this reaction. Although MPW1K is slightly closer to the experimental value (which is very approximate) and the high-level calculations, we chose MPWB1K/6-31+G(d,p) for use in the VTST dynamics calculations for all reactions studied here because of MPWB1K's better performance on broader test sets, as shown in Tables 6 and 12 of ref 42. In any event, the difference in the zero-point-inclusive barrier heights evaluated at the saddle point for these two methods of calculating the surface is only 0.17 kcal/mol. The values of the four energetic parameters calculated at the MPWB1K/DIDZ level are listed in Table 2 for reactions R1, R5, and R7.

Table 2. Energetic Parameters (in kcal/mol) for Reactions R1, R5, and R7 Calculated at the MPWB1K/DIDZ Level[a]

	R1	R5	R7s	R7p1	R7p2
ΔE	0.32	−4.12	−7.66	−3.88	−3.88
ΔH_0	−0.85	−5.43	−8.98	−5.08	−5.08
	(−1.49)[b]	(−5.73)	(−7.74)	(−5.35)	(−5.35)
$V^{\ddagger}$	14.39	11.67	9.47	11.90	11.62
$\Delta V_a^{G\ddagger}$	12.06	8.94	6.52	9.16	9.21

[a] In the case of reaction R7, different energetic parameters are obtained for the abstraction of secondary, R7s, or primary, R7p1 and R7p2, hydrogens and also for each of the two possible transition-state conformers (R7p1 and R7p2) for the primary case (see Section 5.3 of text). [b] Numbers in parentheses are ΔH_{298} from experiment.[41]

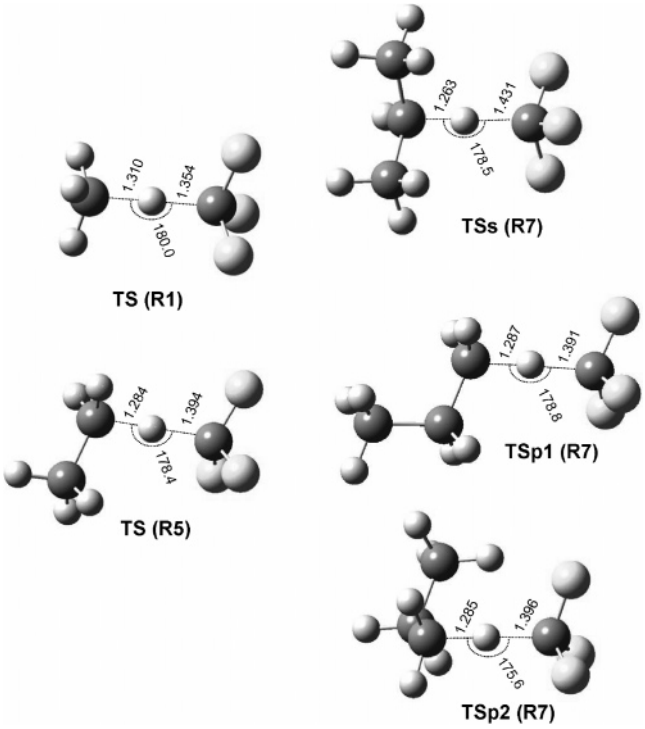

Figure 1. Geometries of the transition states of the R1, R5, and R7 reactions calculated at the MPWB1K/DIDZ level. Distances are in Å, and angles are in degrees.

The geometries of the transition states of reactions R1, R5, and R7 obtained at the MPWB1K/G-31+G(d,p) level are displayed in Figure 1. The transition state for reaction R1 is the only one of the three in which the hydrogen and carbon atoms directly involved in the abstraction are collinear. From the energetic point of view, reactions R5 and R7p are similar, and this is also reflected in the C−H distances of the abstracted hydrogen, which are also similar. Reaction R7s is the one with the lowest barrier and is the most exothermic, and in keeping with Hammond's postu-

late,[45] the transition state is closer to the reactants than it is for the other transition states.

3. Dynamics Calculations

All dynamics calculations were performed by VTST/MT.[9,22,23] This theory minimizes the error due to recrossing trajectories by locating the transition-state dividing surface[46,47] orthogonal to the MEP at a position s along the MEP at which the flux through this surface is minimum, where s is the arc length along the MEP measured from the saddle point. For assigning numerical values of s, all coordinates are scaled to a reduced mass of 1 amu. The set of dividing surfaces over which the flux is minimized is known as the set of generalized transition states[22,23] (GTs). When the flux is minimized for a canonical ensemble, we obtain canonical variational theory (CVT), in which the thermal rate constant, $k^{\mathrm{CVT}}(T)$, at temperature T is the minimum of the generalized transition-state theory rate constant, $k^{\mathrm{GT}}(T,s)$, as a function of s, that is,

$$k^{\mathrm{CVT}}(T) = \min_s k^{\mathrm{GT}}(T,s) = \sigma\frac{k_{\mathrm{B}}T}{h}\frac{Q^{\mathrm{GT}}(T,s_*^{\mathrm{CVT}})}{\Phi^{\mathrm{R}}(T)}\exp[-V_{\mathrm{MEP}}(s_*^{\mathrm{CVT}})/k_{\mathrm{B}}T] \quad (2)$$

where k_{B} is the Boltzmann's constant, h is Planck's constant, σ is the symmetry factor that accounts for the reaction path multiplicity, s_*^{CVT} is the value of s at which the generalized transition-state theory rate constant is a minimum, $V_{\mathrm{MEP}}(s_*^{\mathrm{CVT}})$ is the value of the MEP potential at s_*^{CVT}, $Q^{\mathrm{GT}}(T,s_*^{\mathrm{CVT}})$ is the internal quantum partition function at s_*^{CVT}, and $\Phi^{\mathrm{R}}(T)$ is the product of the relative translational partition function per unit volume and the internal quantum mechanical partition functions of reactants. Both Q^{GT} and Q^{R} are calculated without overall-rotational symmetry numbers, since symmetry is in the σ factor. The internal partition functions are products of the electronic, rotational, and vibrational partition functions, and their zero of energy is at the minimum of the potential, not at the zero-point level. The rotational partition function is approximated as classical, and the vibrational one is a product of separable-mode contributions:

$$Q_{\mathrm{vib}}^{\mathrm{GT}}(T,s) = \prod_{m=1}^{F-1} Q_{\mathrm{vib},m}^{\mathrm{GT}}(T,s) \quad (3)$$

where $F = 3N - 6$ and N is the number of atoms. The partition functions for all the vibrational degrees of freedom except the lowest-frequency mode are quantal harmonic oscillators. For the reactions studied here, the lowest-frequency mode (labeled below as $F - 1$) corresponds to the 3-fold internal rotation of the methyl, ethyl, or propyl group with respect to the CF_3 group and is treated as a hindered rotor. Specifically, the following function is used:

$$V_{\mathrm{vib},F-1}^{\mathrm{GT}}(T,s) = Q_{F-1}^{\mathrm{HO}}(T,s)\tanh\left[\frac{\hbar\omega_{F-1}(s)}{k_{\mathrm{B}}T}Q_{F-1}^{\mathrm{FR}}(T,s)\right] \quad (4)$$

where $\omega_{F-1}(s)$ is the frequency of the internal rotational mode, $Q^{\mathrm{HO}}(T,s)$ is the harmonic oscillator partition function of this mode, given by

$$Q_{F-1}^{\mathrm{HO}}(T,s) = \frac{\exp[-\hbar\omega_{F-1}(s)/2k_{\mathrm{B}}T]}{1-\exp[-\hbar\omega_{F-1}(s)/k_{\mathrm{B}}T]} \quad (5)$$

and $Q^{\mathrm{FR}}(T,s)$ is the free rotor partition function given by

$$Q_{F-1}^{\mathrm{FR}}(T,s) = \frac{[2\pi\, I(s)\, k_{\mathrm{B}}T]^{1/2}}{\hbar\sigma_{F-1}} \quad (6)$$

where σ_{F-1} is the symmetry number for internal rotation (3 for all reactions studied here) and $I(s)$ the reduced moment of inertia of the two counter rotating tops. We use the method[48] (called CW, where C denotes "curvilinear") in which $I(s)$ is obtained from a curvilinear-coordinate description[49] of the torsion and W, which is the barrier for internal rotation, is obtained from electronic structure calculations in which the other degrees of freedom are relaxed while the internal rotation angle is scanned. The frequency, $\omega_{F-1}(s)$ is obtained from the equation

$$\omega_{F-1} = [W_{F-1}/2I(s)]^{1/2}\sigma_{F-1} \quad (7)$$

Because the barrier is very small for these reactions, the partition function for mode $F - 1$ is close to the free-internal-rotor limit.

Tunneling is incorporated into the rate constant by a ground-state transmission coefficient,[9,22,23] $\kappa^{\mathrm{CVT/G}}(T)$, so the final thermal rate constant is given by

$$k^{\mathrm{CVT}/\mu\mathrm{OMT}}(T) = \kappa^{\mathrm{CVT/G}}(T)\, k^{\mathrm{CVT}}(T) \quad (8)$$

Depending on the approximation used in the evaluation of the ground-state tunneling probability, $P^{\mathrm{G}}(E)$, different transmission coefficients for tunneling are obtained. As mentioned in the Introduction, a reliable method to evaluate tunneling effects is the microcanonical optimized multidimensional tunneling transmission factor $\kappa^{\mathrm{CVT}/\mu\mathrm{OMT}}(T)$, for which the probability is obtained as

$$P^{\mu\mathrm{OMT}}(E) = \max\begin{Bmatrix} P^{\mathrm{SCT}}(E) \\ P^{\mathrm{LCT}}(E) \end{Bmatrix} \quad (9)$$

where E is the tunneling energy and $P^{\mathrm{SCT}}(E)$ and $P^{\mathrm{LCT}}(E)$ are the transmission probabilities obtained by the centrifugal-dominant small-curvature semiclassical adiabatic ground state (also called SCT) approximation[8,25] and the large curvature approximation version 4 (LCG4, also called LCT) method,[26] respectively. We will also briefly consider the zero-curvature tunneling[15,22] (ZCT) approximation, which may be considered to be an approximation of SCT in which tunneling occurs along the MEP. An important quantity in all these tunneling theories is the vibrationally adiabatic ground-state potential curve given by

$$V_{\mathrm{a}}^{\mathrm{G}}(s) = V_{\mathrm{MEP}}(s) + \frac{1}{2}\hbar\sum_{m=1}^{F-1}\omega_m(s) \quad (10)$$

where $\omega_m(s)$ are the generalized-normal-mode vibrational frequencies[22,23] at the point that is a distance s along the MEP.

The maximum value of $V_a^G(s)$ is $V_a^{AG}(s)$, and the quantity $\Delta V_a^{G\ddagger}$ discussed above is $V_a^G(s = 0)$ minus $V_a^G(s = -\infty)$.

The LCT probabilities are evaluated along straight-line paths connecting a classical turning point of the vibrationally adiabatic ground-state potential curve on the reactant side ($\tilde{s}_0 < 0$) to a classical turning point of a vibrational potential in the product side ($\tilde{s}_1 > 0$). For ground-state-to-ground-state tunneling, at a given tunneling energy E_{tun}, both turning points satisfy

$$V_a^G(\tilde{s}_i) = E_{tun} \qquad i = 0,1 \tag{11}$$

These points correspond to geometries $\mathbf{x}_0 = \mathbf{x}_{MEP}(\tilde{s}_0)$ and $\mathbf{x}_1 = \mathbf{x}_{MEP}(\tilde{s}_1)$, where $\mathbf{x}$ is a $3N$-dimensional vector specifying the geometry in mass-scaled Cartesian coordinates,[23] also called isoinertial coordinates, and the geometries in isoinertial coordinates along the straight-line tunneling path are

$$\mathbf{x}(\tilde{s}_0,\xi) = \mathbf{x}_0 + \frac{\xi}{\xi_P}(\mathbf{x}_1 - \mathbf{x}_0) \tag{12}$$

where ξ is a progress variable along the tunneling path. The length of the tunneling path is $\xi_P = |\mathbf{x}_1 - \mathbf{x}_0|$. With these definitions, a given tunneling path is specified by $\tilde{s}_0$, and a given point along the straight path is specified by $\tilde{s}_0$ and ξ. At a total energy E, there are contributions from all allowed values of E_{tun} with $E_{tun} \le E$. A value of E_{tun} is not allowed if it is below the zero-point level of either the reactants or products.

In the LCT method, one uses a harmonic approximation to build the effective potential along the straight-line path from the information along the MEP at those points along the tunneling path where (i) all the generalized normal mode coordinates are within their vibrational turning points and (ii) the geometry $\mathbf{x}(\tilde{s}_0,\xi)$ lies within the single-valued region of the reaction-path coordinates. If one of the above conditions is not obeyed, the straight-line path is considered to be in the nonadiabatic region and extrapolation from the MEP is not possible; instead, one evaluates a nonadiabatic effective potential on the basis of the actual potential at a given point of the path and on the contributions of vibrationally adiabatic modes at the adiabatic−nonadiabatic boundaries.[25,26] For a given tunneling path, the nonadiabatic region corresponds to an interval $\xi_I \le \xi \le \xi_{III}$, with ξ_I and ξ_{III} being the boundaries of the adiabatic regions on the reactant and product sides, respectively. The two adiabatic regions, one corresponding to the reactant valley and one to the product valley, are delimited by the intervals $0 < \xi < \xi_I$ and $\xi_{III} < \xi < \xi_P$. The LCG4 transmission coefficients involve an additional condition; that is, the extrapolated vibrationally adiabatic potential obtained from the MEP information should be larger than the calculated nonadiabatic effective potential. The vibrationally adiabatic potential is obtained from information on the MEP, but the evaluation of the nonadiabatic effective potential involves single-point calculations along each tunneling path. The large number of single-point energies required (usually more than 1000) make the evaluation of LCT transmission coefficients time-consuming.

One way of reducing the computational cost is to calculate single-point energies at selected points along the straight-line path at each tunneling energy. The calculated points are fitted to a one-dimensional spline under tension with a subsequent reduction in computer time. This procedure[50] is called one-dimensional spline interpolated large-curvature tunneling (ILCT1D), and it produces converged transmission coefficients with a mean signed percentage error smaller than 4% with only nine calculated points at each tunneling energy.

Another possibility is not only to interpolate in the progress variable ξ at each tunneling energy E_{tun} but also to interpolate in E_{tun}. This two-dimensional interpolation method is presented in the rest of this paragraph and is based on a two-dimensional spline under tension. We called it the ILCT(2D) algorithm. The procedure is as follows: (i) An $M \times N$ two-dimensional grid is defined in terms of the tunneling energies E_i (with $i = 1, ..., M$) at which tunneling is to be evaluated and the points ξ_j (with $j = 1, ..., N$) to be calculated at each of the specified tunneling energies since $\tilde{s}_0$, $\mathbf{x}_0$, and $\mathbf{x}_1$ in eq 12 are functions of E_i. A general point on a straight-line path has coordinates (E_i, ξ_j) and is related to a unique geometry given by eq 12 for each tunneling energy E_i. (ii) The next step is to calculate the potential for the generic point (E_i, ξ_j). If the point is in the adiabatic region, the energy is calculated by a quadratic expansion from the information along the MEP, and so no additional computer time is needed; if the point is in the nonadiabatic region, the classical potential has to be calculated explicitly. It should be noted that a preliminary search is needed in order to know the boundaries between the adiabatic and the nonadiabatic regions. (iii) The initial grid with points (E_i, ξ_j) is transformed in a square grid with points ($\bar{E}_i$, $\bar{\xi}_j$) by performing the following scaling:

$$\bar{E}_i = \frac{E_i - E_{min}}{E_{max} - E_{min}} \text{ and } \bar{\xi}_j = \frac{\xi_j}{\xi_{P,i}} \tag{13}$$

where E_{min} is the lowest tunneling energy at which the particle can tunnel, E_{max} is the maximum V_a^{AG} of the vibrationally adiabatic potential curve, and $\xi_{P,i}$ is the length of the tunneling path at the given tunneling energy E_i. This grid is fitted to a two-dimensional spline under tension. [See Figure 2, where the point corresponding to E_{max} becomes a line when the region from (0, 0) to ($\bar{\xi}_{j_{max}}$, $\bar{E}_{i_{max}}$) is mapped onto a unit square.] (iv) The effective potentials in the swath are then obtained from the fit.

In LCT tunneling calculations by the LCG4 algorithm (or any of the earlier large-curvature algorithms), the tunneling calculation is always carried out in the exoergic direction (as determined for the ground-state-to-ground-state process at 0 K), and transmission coefficients for the other direction are obtained by detailed balance. Tunneling is initiated in the ground state of the reactants (in the exoergic direction) but into a series of ground and excited states of the product (even for thermoneutral regions). The four steps of the previous paragraph are repeated for each of the directly coupled (diabatic) vibrationally excited final states. If only the ground-state product is requested or if the final vibrationally excited states to which the tunneling is directly coupled are not open, the loop is carried out just once.

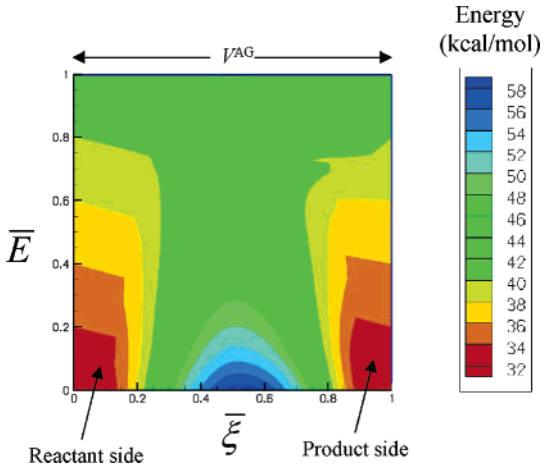

Figure 2. Unit-square potential energy surface evaluated by the ILCT(2D) algorithm using a 9 × 11 grid. The lowest tunneling energy included is 31.11 kcal/mol, and the largest tunneling energy included is 41.73 kcal/mol, which is the maximum of the vibrationally adiabatic ground-state potential curve.

Table 3. Comparison between the Full LCG4 Calculation and Several ILCT(2D) Calculations with $m \times n$ Grids of the LCG4 Transmission Coefficients for Reaction $C_6H_6 + CH_3 \rightarrow C_6H_5 + CH_4$ Using the J1 Potential Energy Surface

$T/m \times n$	full	9 × 11	7 × 9	5 × 9	3 × 5
200	92.1	92.1	88.9	99.3	71.7
250	26.1	26.1	26.1	24.6	21.5
300	12.2	12.2	12.3	10.9	10.3
400	5.07	5.06	5.17	4.50	4.47
500	3.13	3.13	3.20	2.82	2.84
600	2.33	2.33	2.37	2.13	2.16
points[a]	4834	221	205	192	174

[a] This row lists the number of points in the nonadiabatic region that need to be evaluated to obtain the transmission coefficients.

Having obtained the μOMT transmission probability P^G as a function of E, the transmission coefficient is calculated by

$$\kappa^{\mathrm{CVT/Q}} = \frac{\int_{V_a^G(s=-\infty)}^{\infty} e^{-E/k_B T} P^G(E)\, dE}{k_B T \exp[-V_a^G(s_*^{\mathrm{CVT}})/k_B T]} \qquad (14)$$

The energy at which the integrand of the integral in the numerator of this integral has a maximum is called the representative tunneling energy.

To check the accuracy of the ILCT(2D) algorithm, full calculations of the LCT transmission coefficients were carried out, first, for the $C_6H_6 + CH_3 \rightarrow C_6H_5 + CH_4$ reaction using the J1 potential energy surface of the $H_2 + CH_3 \rightarrow H + CH_4$ reaction but with a fictitious mass of 77 amu (mass of C_6H_5) for the donor atom. This reaction is used to show the performance of the ILCT(2D) algorithm when tunneling effects are larger. Results for this reaction are given in Table 3, which shows that excellent performance is obtained when a grid of 99 points is used (11 points along the straight-line tunneling path for tunneling paths corresponding to nine different tunneling energies, with $\bar{\xi}_j$ and $\bar{E}_i$ given by eq 13). Similar tests were carried out for reaction R2, and again, 99 points suffice, as shown in Table 4.

Table 4. LCT Transmission Coefficients for the R2 Reaction Obtained by Using a Grid of 80 × 180 Points (Full-LCT) and the ILCT(2D) Algorithm with a 9 × 11 Grid

T (K)	full LCT	ILCT(2D)
200	75.6	75.9
300	6.82	6.83
400	2.98	2.98
500	2.02	2.02
600	1.63	1.63
700	1.44	1.44

The ILCT(2D) algorithm is implemented in the program POLYRATE 9.3.1.[51] All dynamics calculations were carried out with the program GAUSSRATE 9.1,[52] which was used to provide an interface between GAUSSIAN03[53] and POLYRATE 9.3.1.

4. Dynamics Details

All available experimental measurements of the thermal rate constants of the hydrogen abstraction reactions R1−R8 are relative to the high-pressure limit of the radical recombination rate constant for the reaction $2CF_3 \rightarrow C_2F_6$. To do a direct comparison of our calculated rate constants with those of the experiment, it is necessary to know this rate constant, called $k_{r,\infty}$. Here, we use the value inferred previously,[9] in particular, $k_{r,\infty} = 3.9 \times 10^{-11}$ (cm^3 molecule^{-1}) exp[−1.36 (kcal/mol)/RT].

All dynamics calculations were carried out at the MPWB1K/DIDZ level. To carry out the VTST/MT calculations using μOMT transmission coefficients for tunneling, information about the potential is needed along the MEP and in the reaction swath. The MEP was followed using the Page−McIver algorithm[54] with a step size of 0.01 a_0 and a scaling mass $\mu = 1$ amu; Hessian calculations were saved every nine steps. The dividing surface was defined in terms of redundant internal coordinates.[55] All frequencies were scaled by a factor[38] of 0.9537. The reaction swath was covered by 80 straight-line paths starting and ending at the classical turning points that obey eq 11. The evaluation of the LCT tunneling probabilities for each path (or tunneling energy) required 180 single-point energy calculations to characterize the potential. Since the integral over total energy[56] was carried out by 80-point quadrature, this procedure requires 14 400 single-point calculations for the evaluation of ground-state LCT tunneling probabilities. In addition, for any final vibrational excited-state included, a new set of 14 400 points is needed. As explained above, each set of 14 400 points was obtained by interpolation from a 99-point grid.

The grid for the 2D spline-under-tension calculation on R2 is plotted in Figure 2. For both the full-LCT and the ILCT(2D) methods, single-point calculations are needed only at the boundaries and at points of the grid inside those boundaries. The amount of time that is saved using ILCT(2D) with respect to full-LCT for reactions R2, R5, and R7 is indicated in Table 5. A full-LCT calculation involves 30 times more computer time than the ILCT(2D) calculation but gives similar results. Hereafter, for all reactions, the LCT transmission coefficients were obtained with the ILCT(2D) algorithm.

Table 5. Number of Single-Point Calculations and Computer Time Required for the Evaluation of the LCT Transmission Coefficients by Full Calculation (First Two Numerical Rows) and by the ILCT(2D) Procedure (Third and Fourth Numerical Rows) for Reactions R2, R5, and R7

	R2	R5	R7
full-LCT			
number of points	3370	1827	920
computer time[a] (s)	566 160	678 163	444 960
ILCT(2D)			
number of points	113	70	69
computer time[a] (s)	18 984	25 830	33 672

[a] Calculations carried out on a 3 GHz Pentium 4 PC.

Table 6. Barrier W_{F-1} and Frequency (Obtained from eq 8) ω_{F-1}, Both in cm^{-1}, for the Internal Rotation around the C−C Axis at the Transition State for Reactions R1−R8

	W_{F-1}	ω_{F-1}		W_{F-1}	ω_{F-1}
R1	10.4	22.2	R7s	38.1	12.4
R2	10.4	16.0	R7p1	16.5	10.8
R3	10.4	17.5	R7p2	54.2	14.3
R4	10.4	16.0	R8s	38.1	11.4
R5	23.8	14.0	R8p1	16.5	9.4
R6	23.8	12.2	R8p2	54.2	13.3

5. Calculations, Results, and Discussion

Internal Rotation. The transition state obtained by MPWB1K/DIDZ for reactions R1−R4 have C_3 symmetry, and the fluorine atoms of the CF_3 group and the H atoms of the CH_3 group are in a nearly trans conformation with a FCCH dihedral angle of 178.0 degrees (see Figure 1). The internal rotation of CH_3 with respect to the CF_3 group is almost free and has a rotational barrier of only 10.4 cm^{-1}. The frequency of internal rotation was calculated from eq 7. The reduced moment of inertia is calculated using the CW model.[48] All frequencies for internal rotation for reactions R5−R8 were also calculated by this procedure, and the results are shown in Table 6.

The hindered rotor partition functions for $CF_3 + CH_4$ are 10% less than the free rotor value at 300 K and 5% less than the free rotor value at 700 K. For propane, these percentages range from 8 to 21% at 300 K and 3−10% at 700 K, depending on the conformation.

5.1. CF_3 + Methane. Dynamics. The MEPs for reactions R1−R4 were calculated in the interval $s = -6.5$ to 3.5 a_0. The vibrationally adiabatic ground-state potential energy curves for reactions R1−R4 are plotted in Figure 3. None of the four reactions has a variational effect (i.e., the variational transition state passes through the saddle point), and therefore, the CVT rate constants for these four reactions are equal to those obtained by conventional transition-state theory (TST); that is, eq 8 reduces to

$$k^{\mathrm{TST}/\mu\mathrm{OMT}}(T) = k^{\mathrm{TST/G}}(T)\, k^{\mathrm{TST}}(T) \qquad (15)$$

To obtain $k^{\mathrm{TST}}(T)$, only information at the stationary points (reactants and transition state) is needed. However, the evaluation of the transmission coefficient requires information along the MEP and in the swath.

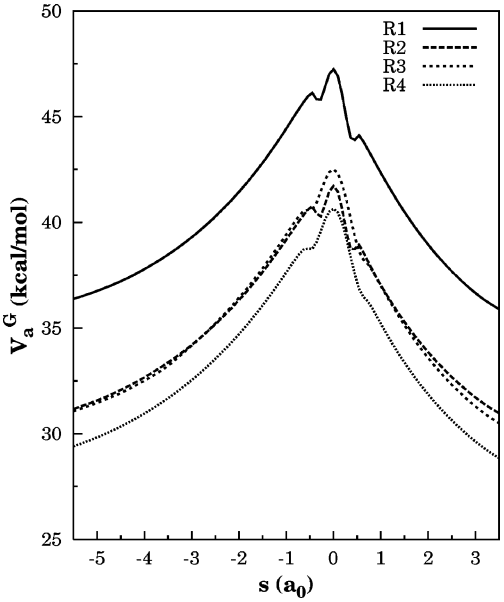

Figure 3. Vibrational adiabatic potential for reactions R1−R4.

The symmetry number of the reaction, which was already introduced in eq 2, is given by the product of the symmetry number of reactants divided by the symmetry number of the transition state. Since $\sigma(CF_3) = 3$, $\sigma(CH_4) = 12$, $\sigma(CD_3H) = 3$, σ(TS of R1, R2, and R4) = 3, and σ(TS of R3) = 1, the symmetry numbers for reactions R1, R2, R3, and R4 are 12, 3, 9, and 12, respectively.

If the internal rotation were treated as a harmonic vibration, the absolute rate constants for R1 would be 2.66 and 3.94 times larger, at temperatures of 300 and 700 K, respectively, than those obtained if eq 4 is used. This shows, in agreement with ref 9, that anharmonicity is significant.

It would be expected that tunneling is more important for reactions R1 and R2 than for reactions R3 and R4, because a hydrogen atom is transferred for the first two reactions whereas, for the latter, the transferred atom is a deuterium, which is heavier. The vibrationally adiabatic ground-state potential energy curves for these four reactions are plotted in Figure 3. A parameter that is sometimes used to indicate the importance of tunneling is the imaginary frequency at the saddle point; a larger imaginary frequency indicates a narrower barrier along the MEP or a lighter tunneling mass. The imaginary frequency is larger for reactions R1 and R2, with values of 1697i cm^{-1} and 1685i cm^{-1}, respectively, than for reactions R3 and R4, which have values of 1247i cm^{-1} and 1243i cm^{-1}, respectively. A more quantitative assessment of tunneling requires multidimensional methods that incorporate the coupling between the reaction coordinate and the $3N - 7$ orthogonal normal modes, that is, coupling to modes transverse to (perpendicular to) the reaction coordinate. Tunneling was evaluated by both the SCT and LCT approximations to obtain the μOMT transmission coefficients, and calculations with the ZCT approximation were carried out for comparison. The ZCT, SCT, LCT, and μOMT multidimensional transmission coefficients are listed in Table 7. The ZCT, SCT, and LCT approximations all include multidimensional effects, but to different extents. The ZCT

Table 7. Tunneling Transmission Coefficients for Reactions R1−R4 Obtained by Multidimensional Tunneling Approximations

reaction	*T*(K)	ZCT	SCT	LCT	μOMT
R1	200	13.8	101	319	329
	300	3.57	9.18	9.60	11.0
	400	2.12	3.69	3.42	3.92
	500	1.64	2.37	2.18	2.43
	600	1.42	1.84	1.71	1.87
	700	1.30	1.57	1.49	1.59
R2	200	10.5	62.7	75.6	84.0
	300	3.14	7.40	6.83	7.90
	400	1.97	3.27	2.98	3.36
	500	1.56	2.18	2.02	2.22
	600	1.37	1.74	1.63	1.76
	700	1.26	1.51	1.44	1.52
R3	200	13.8	72.3	61.9	85.4
	300	3.31	6.52	4.60	6.68
	400	1.97	2.85	2.22	2.86
	500	1.55	1.95	1.64	1.95
	600	1.36	1.59	1.41	1.59
	700	1.25	1.40	1.28	1.40
R4	200	13.1	65.3	58.0	79.4
	300	3.23	6.29	4.49	6.47
	400	1.95	2.80	2.20	2.82
	500	1.54	1.93	1.63	1.93
	600	1.35	1.58	1.40	1.58
	700	1.25	1.40	1.28	1.40

approximation includes coupling of the reaction coordinate to orthogonal degrees of freedom in that it includes the s variation of the generalized normal-mode frequencies $\omega_m(s)$, but it does not include corner cutting. The SCT approximation includes the s variation of $\omega_m(s)$ plus the small-curvature limit of corner cutting. Note that the s variation of $\omega_m(s)$ results from coupling in the potential energy, and corner cutting results from coupling in the kinetic energy. The LCT approximation also includes both of these couplings, and furthermore, it allows for extreme corner cutting.

For reactions R1 and R2, the μOMT transmission coefficients are larger than the SCT transmission coefficients at low temperatures, and this results from extreme corner-cutting contributions at low tunneling energies. For reactions R3 and R4, the SCT and μOMT transmission coefficients are similar, indicating a tunneling path closer to the MEP. It is clear from these results that although the LCT paths may be unimportant for deuterium transfer and for hydrogen transfer at high temperatures (for the reactions under discussion here), they play an important role for hydrogen transfer at low temperatures. The consequence is that, for systems of this type, a tunneling evaluation based exclusively on the SCT transmission coefficients may underestimate the thermal rate for hydrogen transfer and, therefore, may lead to a wrong kinetic isotope effect (KIE). Neglecting corner cutting completely, as in the ZCT approximation, leads to even larger errors, with the largest error being more than a factor of 3 at 300 K and an order of magnitude at 200 K.

Another important aspect to consider is the contribution to the rate constants due to tunneling directly into final

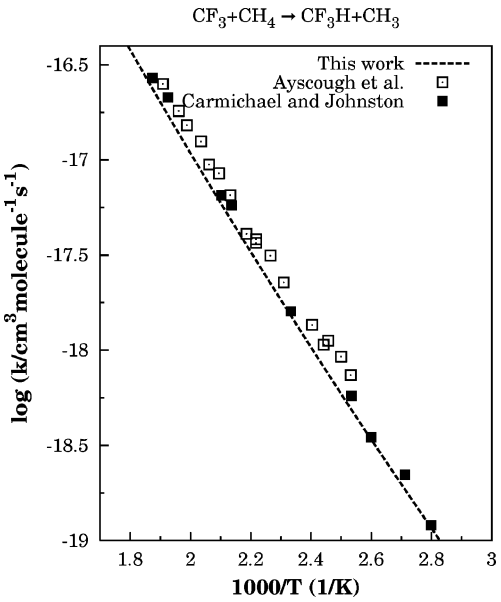

Figure 4. Arrhenius plot for reaction R1.

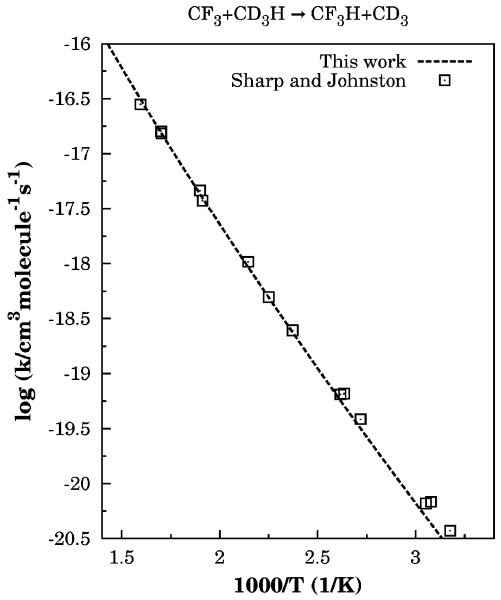

Figure 5. Arrhenius plot for reaction R2.

excited vibrational states, which is allowed only in the LCT approximation. However, in these cases, such contributions due to excited vibrational states are negligible.

The thermal rate constants for reactions R1−R4 are plotted in Figures 4−7 and are given in tables in the Supporting Information. The calculated TST/μOMT thermal rate constants are in good agreement with the experimental values for reactions R1, R2, and R4, but the calculated values for reaction R3 are much too high.

To understand the KIEs better, we factored them as follows. We denote the calculated KIE as η, and we first factor this, on the basis of eq 14, into tunneling and overbarrier contributions:

$$\eta = \eta_{\text{tun}}\eta_{\text{TST}} \tag{16}$$

One should note here, in justifying the subscript "tun", that the transmission coefficients include both tunneling and

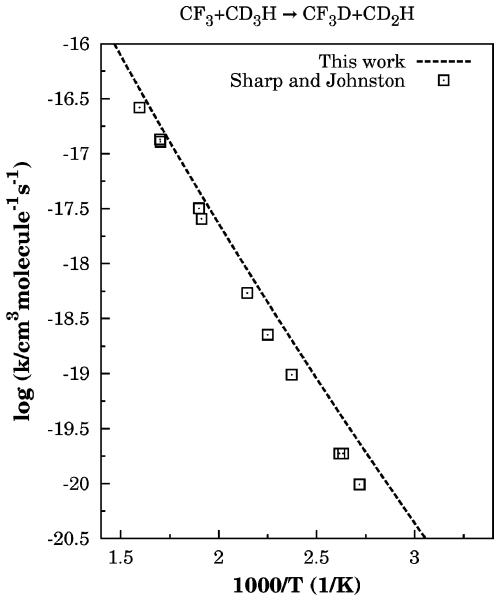

Figure 6. Arrhenius plot for reaction R3.

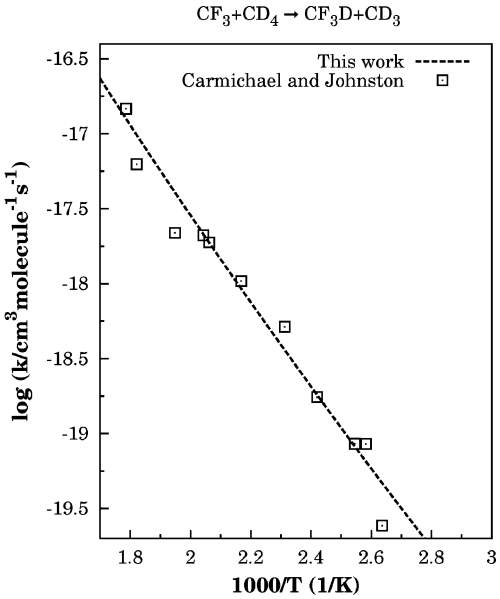

Figure 7. Arrhenius plot for reaction R4.

nonclassical reflections,[23,56] and so technically, they include both these quantum effects on the reaction-coordinate motion, but we usually simply discuss the net effect and call it tunneling, which is usually the dominant of the two effects. The result obtained with classical reaction-coordinate motion and quantized vibrations is also called the quasiclassical (QC) contribution; for the four reactions R1−R4, this is η_{TST}. We factor this into translational, rotational, and vibrational contributions:

$$\eta^{QC} = \eta_{TST} = \eta_{trans}\eta_{rot}\eta_{vib} \qquad (17)$$

Note that η_{trans} and η_{rot} are independent of temperature. Table 8 shows the factors for $\eta = k_{R1}/k_{R4}$ and for $\eta = k_{R2}/k_{R3}$. (Results at more temperatures are in the Supporting Information.) Theory predicts KIEs a little smaller than the experimental values. It is not clear if this presents a challenge for theory or if it indicates inaccuracies in the experiment.

Table 8. Factors in the KIEs

T (K)	η_{tun}	η_{vib}	η^{QC}	η	η_{exp}
		R1/R4[a]			
300	1.71	1.82	5.77	9.83	n.a.[b]
400	1.39	1.22	3.89	5.40	6.2[c]
500	1.26	0.96	3.02	3.80	6.0[c]
700	1.14	0.71	2.25	2.56	n.a
		R2/R3[d]			
300	1.18	4.22	4.39	5.18	n.a.
400	1.17	3.06	3.18	3.72	8.5[e]
500	1.11	2.5	2.61	2.98	5.0[e]
700	1.09	1.98	2.06	2.25	n.a

[a] $\eta_{trans} = 1.31$; $\eta_{rot} = 2.42$. [b] n.a. denotes not available. [c] Interpolated from ref 31. [d] $\eta_{trans} = 1.00$; $\eta_{rot} = 1.04$. [e] Interpolated from ref 29.

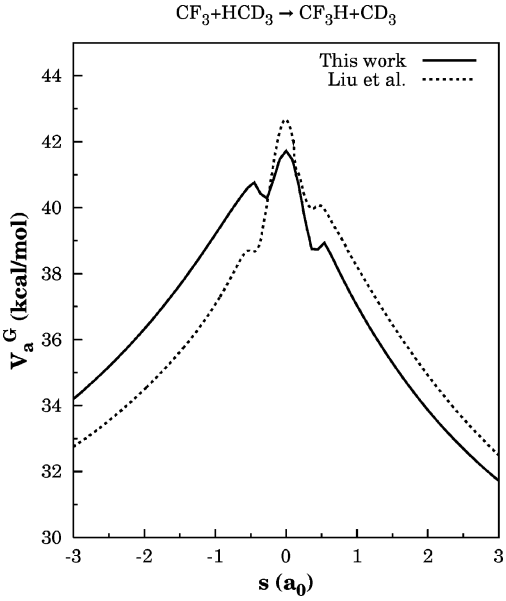

Figure 8. Comparison of vibrationally adiabatic ground-state potential curves obtained in this work and that of Liu et al.[23]

There are some important differences between the present results and those in the previous[9] CF_3 paper. The first difference is that no variational effects are observed in the present work, and the second is that the contribution due to tunneling is much smaller. Figure 8 shows a comparison between the present and previous calculations of the vibrationally adiabatic ground-state potential curve. The MPWB1K and MPW1K levels of calculation lead to imaginary frequencies of 1697i and 1694i cm^{-1}, respectively, whereas the previous AM1-SRP2 calculations led to an imaginary frequency of 2113i cm^{-1}, indicating that the effective potential along the MEP is thinner. An additional factor contributing to the narrower vibrationally adiabatic ground-state potential curve in the previous calculation is that it was obtained in Cartesian coordinates, which usually yields an artificially narrow effective potential as compared to that obtained in the more physically redundant internal coordinates. The present effective potential would be expected to be more realistic not only because of the more physical coordinate system but also because density functionals with one parameter optimized for kinetics are generally more reliable than AM1 for hydrogen atom transfer reactions.[42,57]

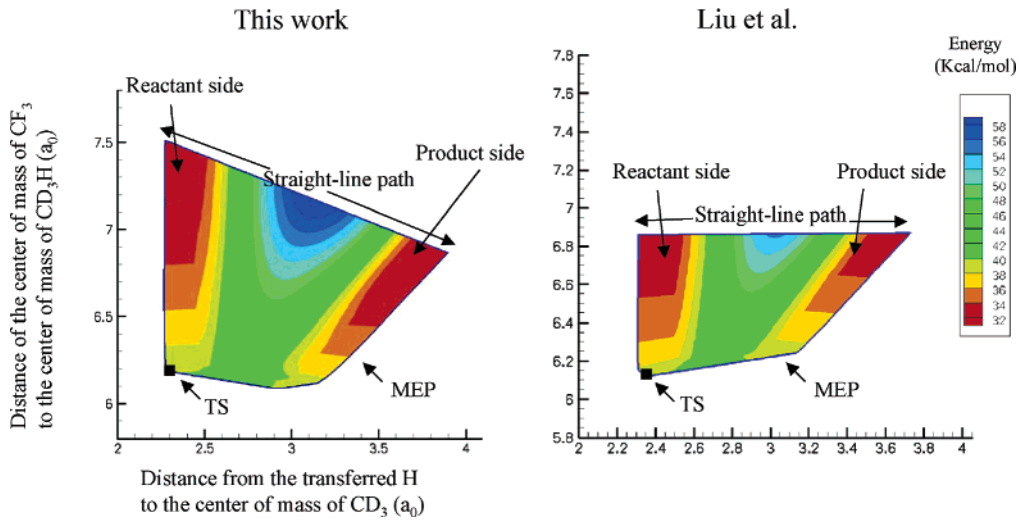

Figure 9. Plot of the effective potential for ground-state tunneling along the MEP and in the reaction "swath" in mass-scaled pseudo-Jacobian coordinates for reaction R2. The effective potential equals the vibrationally adiabatic ground-state potential in the adiabatic region. The left-side contours were obtained in the present work at the MPWB1K/6-31+G(d,p) level, and the lowest tunneling energy included is 31.11 kcal/mol. The right-side contours are those obtained using the AM1-SRP2 method described by Liu et al.,[23] and the lowest tunneling energy included is 32.11 kcal/mol. In both cases, the location of the TS is marked with a black square.

Table 9. Imaginary Frequency, $\omega^{\ddagger}$ (in cm^{-1}), and Energetic Parameters (in kcal/mol) for Reaction R2 Calculated at the AM1-SRP2 and MPWB1K/DIDZ Levels

	AM1-SRP2	MPWB1K
$V^{\ddagger}$	14.63	14.39
ΔE	−0.74	0.32
$\Delta V_a^{G\ddagger}$	12.40	12.06
ΔH_0	−1.19	−0.85
$\omega^{\ddagger}$	2113i	1697i

Table 10. Transmission Coefficients for Reactions R2 and R3

		Liu et al.[a]			this work[b]		
reaction	T (K)	SCT	LCT	μOMT	SCT	LCT	μOMT
R2	367.8	8.0	17.0	18.0	3.98	3.62	4.13
	626.8	2.2	2.6	2.7	1.66	1.57	1.68
R3	367.8	4.0	6.7	7.8	3.46	2.61	3.49
	626.8	1.8	1.7	1.8	1.53	1.36	1.53

[a] AM1-SRP2.[9] [b] MPWB1K/DIDZ.

Nevertheless, one cannot discount the possibility that the MPWB1K/DIDZ method overestimates the width of the barrier (and that such an overestimate adversely affects the agreement with experimental results). The surface properties are further compared in Table 9. Figure 9 compares the effective potentials in the swath. Note that for both cases shown in the figure, the lowest energy shown is the lowest energy actually used in the calculations, and the tunneling probability is negligible at this energy. In the MPWB1K case, V_a^{AG} is 41.73 kcal/mol, and the lowest energy considered is 10.62 kcal/mol below this. In the AM1-SRP2 case, V_a^{AG} is 42.65 kcal/mol, and the lowest tunneling energy considered is 10.54 kcal/mol below this. Tables 10 and 11 compare the representative tunneling energies and transmission coefficients for the two sets of calculations; tunneling is significant down to lower energies in the previous study.

Table 11. Representative Tunneling Energies (in kcal/mol) for Reaction R2

		Liu et al.[a]			this work		
reaction	T (K)	SCT	LCT	μOMT	SCT	LCT	μOMT
R2	367.8	40.1	38.7	38.7	40.5	40.8	40.8
	626.8	41.5	40.2	41.5	40.8	40.8	40.8

[a] Ref 9.

Table 12. KIEs and Their Factors for Reactions R2 and R3

	Liu et al.[9]			this work		
T (K)	η_{tun}	η^{QC}	η	η_{tun}	η^{QC}	η
367.8	2.3	4.0	9.1	1.18	3.48	4.11
626.8	1.5	2.0	3.0	1.10	2.22	2.44

The consequences of these differences are shown in Table 12; the present calculations predict much smaller KIEs.

The differences of the transmission coefficients from the two calculations that are compared in Table 12 are not due entirely to the differences in the potential energy surfaces. Another source of difference is that ref 9 used the LCG3 approximation for the LCT transmission probabilities, whereas the present article used the LCG4 approximation. Repeating the AM1-SRP2 calculations with LCG4 lowers the LCT transmission coefficients for R2 to 11.7 and 2.4 at 367.8 and 626.8 K. The results with LCG4 are closer to the present results for R2, but there is less difference between LCG3 and LCG4 for R3. We conclude that both the potential energy surface and the tunneling approximation contribute to the differences of ref 9 from the present work.

5.2. CF_3 + Ethane. As in the case of reactions R1−R4, reactions R5 and R6 do not show variational effects, and the final variational transition-state theory rate constant is given by eq 15. The symmetry numbers are $\sigma(CF_3) = 3$, $\sigma(C_2H_6) = 6$, $\sigma(C_2D_6) = 6$, and σ(TS of R5 and R6) = 1.

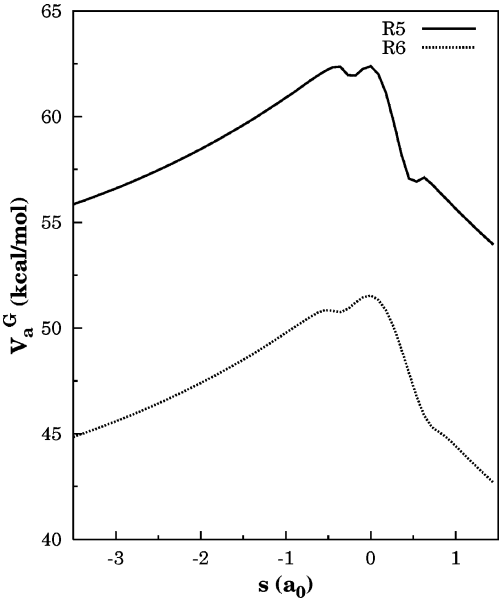

Figure 10. Vibrational adiabatic potential for reactions R5 and R6.

Table 13. SCT, LCT, and μOMT Transmission Factors, κ, for the H and D Abstraction by CF_3 of H(D) Atoms of Ethane

	R5			R6		
T (K)	κ^{SCT}	κ^{LCT}	$\kappa^{\mu OMT}$	κ^{SCT}	κ^{LCT}	$\kappa^{\mu OMT}$
300	3.18	2.19	3.20	3.24	2.34	3.27
400	1.91	1.47	1.91	1.95	1.57	1.95
500	1.51	1.26	1.51	1.54	1.33	1.54
600	1.33	1.17	1.33	1.35	1.21	1.35
700	1.23	1.12	1.23	1.25	1.15	1.25

The lowest-frequency mode, as in the previous case, is treated by the CW approximation, which decreases the rate constant, as compared to a harmonic calculation, by a factor of 1.9 at $T = 300$ K and a factor of 2.7 at $T = 700$ K. The imaginary frequencies for reactions R5 and R6 are 1618i cm^{-1} and 1190i cm^{-1}, respectively. The classical barrier height for this reaction is lower than that for the reaction of CF_3 with methane (see Table 2), and the fractional contribution due to tunneling is smaller, although the reaction still proceeds mainly by tunneling. In particular, the SCT and LCT4 transmission coefficients for reaction R5 at 300 K are 3.17 and 2.18, respectively. The μOMT transmission coefficient at this temperature is 3.20, indicating that tunneling is well-represented by the SCT approximation in the range of temperatures studied. Table 13 shows that the tunneling is mainly of the small-curvature type at 400−700 K as well.

Figure 10 shows that the vibrationally adiabatic potential has two similar maxima, one at $s = -0.40$ and one at $s = 0$ a_0. This indicates that the reaction has two bottlenecks and that both of them should be taken into account in the evaluation of the thermal rate constants. The canonical unified statistical theory[23,58] transmission coefficient Γ_{CUS} incorporates this second bottleneck and is given by

$$\Gamma^{CUS}(T) = [1 + q_{vr}^{CVT}(T)/q_{vr}^{max}(t) - q_{vr}^{CVT}(T)/q_{vr}^{min}(T)]^{-1} \quad (18)$$

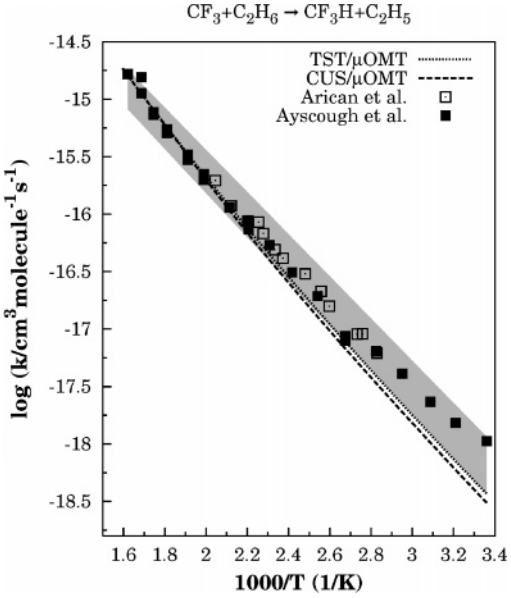

Figure 11. Arrhenius plot for reaction R5. The gray area indicates the standard deviation reported by Arican and Arthur.[32]

where

$$q_{vr}^{CVT}(T) = Q_{vr}^{GT}(T,s_*^{CVT}) \exp[-\beta V_{MEP}(s)] \quad (19)$$

with $Q_{vr}^{GT}(T,s_*^{CVT})$ being evaluated at the absolute maximum of the free energy (which in this case coincides with $s = 0$, because there is no variational effect); $q_{vr}^{max}(T)$ is evaluated at the second highest maximum in the free energy, and $q_{vr}^{min}(T)$ is evaluated at the lowest minimum between the two maxima. The resulting $k^{CUS/\mu OMT}$ rate constant is given by

$$k^{CUS/\mu OMT}(T) = \Gamma^{CUS}(T)\, k^{CVT/\mu OMT} \quad (20)$$

For instance, at $T = 300$ K, the highest maximum in the free energy is located at $s = 0$, where the generalized free energy of activation[22,23] is 45.14 kcal/mol, and the second largest maximum is at $s = -0.37$ a_0 where it is 44.77 kcal/mol, whereas the minimum is located at $s = -0.25$ a_0, where the generalized free energy of activation is 44.50 kcal/mol. From these data, one obtains $R_{CUS}(T = 300\ K) = 0.83$. The value of R_{CUS} becomes unity at temperatures above 510 K. Reaction R6 has only one bottleneck, which is at $s = 0$, and therefore, in this case,

$$k^{CUS/\mu OMT}(T) = k^{CVT/\mu OMT}(T) = k^{TST/\mu OMT}(T) \quad (21)$$

The rate constants are plotted in Figure 11 and tabulated in the Supporting Information.

The TST KIEs, η, were factored using eqs 16 and 17. More generally,

$$\eta = \eta_{trans}\eta_{rot}^{TST}\eta_{vib}^{TST}\eta_{var}\eta^{CUS}\eta_{tun} \quad (22)$$

The product $\eta_{trans}\eta_{rot}^{TST}\eta_{vib}^{TST}$ equals η_{TST}, which is the KIE

Table 14. Factorization of the KIE k(R5)/k(R6)

T (K)	η_{vib}^{TST}	η_{TST}	η^{CUS}	η^{QC}	η_{tun}	η
300	2.79	5.75	0.83	4.76	0.98	4.67
400	1.84	3.82	0.88	3.35	0.98	3.29
500	1.43	2.97	0.91	2.70	0.98	2.65
700	1.07	2.22	1.00	2.22	0.99	2.18

predicted by conventional TST. The KIE due to variational effects, η_{var}, is calculated as

$$\eta_{var} = \frac{k_H^{CVT}(T)\, k_D^{TST}(T)}{k_D^{CVT}(T)\, k_H^{TST}(T)} \tag{23}$$

(Note that η_{rot}^{TST} and η_{vib}^{TST} are not the full rotational and vibrational effects; those would be obtained by also factoring η_{var} into contributions from vibrational and rotational modes.) The KIE due to the recrossing included in CUS theory is

$$\eta_{CUS} = \frac{\Gamma_H^{CUS}(T)}{\Gamma_D^{CUS}(T)} \tag{24}$$

The TST, variational, and CUS contributions may be combined into a quasiclassical contribution such that

$$\eta^{QC} = \eta_{TST}\eta_{var}\eta^{CUS} \tag{25}$$

and

$$\eta = \eta_{tun}\eta^{QC} \tag{26}$$

where the contribution due to quantum effects is included as the ratio between the μOMT transmission coefficients

$$\eta_{tun} = \frac{\kappa_H^{\mu OMT}(T)}{\kappa_D^{\mu OMT}(T)} \tag{27}$$

These factors are given in Table 14, which shows that the temperature dependence of the KIE is dominated by the vibrations and that tunneling nearly cancels out in the KIE for R5 versus R6. (Results for more temperatures are in the Supporting Information.)

5.3. CF_3 + Propane. For reactions R7 and R8, there are two types of hydrogen/deuterium atoms that can be abstracted: primary (from the terminal methyl groups) and secondary (from the central carbon atom). Thus, we make a distinction between the reactions

$$CF_3 + H_3C{-}CH_2{-}CH_3 \rightarrow CF_3H + H_3C{-}CH_2{-}CH_2 \quad \text{(R7p)}$$

and

$$CF_3 + H_3C{-}CH_2{-}CH_3 \rightarrow CF_3H + H_3C{-}CH{-}CH_3 \quad \text{(R7s)}$$

The transition states for the abstraction of a primary and secondary hydrogen atom are shown in Figure 1.

Propane has C_{2v} symmetry; therefore, $\sigma(C_3H_8) = 2$. Furthermore, $\sigma(CF_3) = 3$, and σ(TS of R7s) = 1; therefore, the symmetry number for the abstraction of a secondary hydrogen, H_s, is 6.

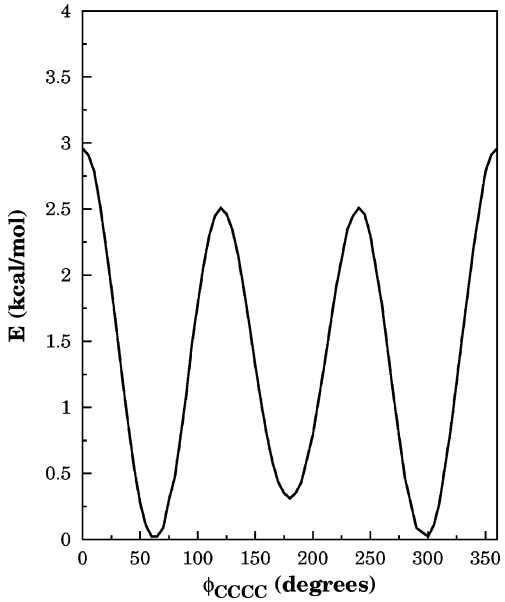

Figure 12. Potential for internal rotation at the TS for reaction R7p.

In the case of abstraction of a hydrogen of the two terminal methyl groups, there are two possibilities: (a) the abstraction of one of the two hydrogen atoms having a dihedral angle $\phi_{HCCC} = 180°$ (we label these hydrogen atoms as H_{p1} and the abstraction reaction as R7p1) and (b) the abstraction of one of the four atoms having dihedral angles of $\phi_{HCCC} = 60°$ (two of them) and $\phi_{HCCC} = -60°$(the other two), and we label these hydrogen atoms as H_{p2} and the abstraction reactions as R7p2. The TS for the hydrogen abstraction of H_{p1} has no symmetry, and therefore, the symmetry number for this reaction is 6. The rotation around the terminal methyl group (see Figure 12) starting from this transition-state structure indicates that there are another two transition states at $\phi_{CCCC} = 62°$and $-62°$, respectively, which cannot be superimposed and which are separated by a barrier of 2.51 kcal/mol. These two transition states correspond to the H_{p2} hydrogen abstractions. Therefore, the symmetry number for the abstraction of the H_{p2} hydrogen abstractions is $\sigma(CF_3) \times \sigma(C_3H_8) \times m^{\ddagger}(TSp) = 12$, with $m^{\ddagger}(TSp) = 2$ because of the two isoenergetic optically active transition states. The imaginary frequencies at the transition states are 1484i, 1630i, and 1619i cm^{-1} for R7s, R7p1, and R7p2, respectively, and 1099i, 1198i, and 1190i cm^{-1} for R8s, R8p1, and R8p2, respectively. The total rate constant for the abstraction of a hydrogen atom from propane by CF_3 can be obtained as the sum of all these contributions, that is,

$$k_{R7}(T) = k_{R7s}(T) + k_{R7p1}(T) + k_{R7p2}(T)$$

The vibrationally adiabatic ground-state potential curves are plotted in Figure 13. As indicated in Table 2, the abstraction of a secondary hydrogen has a barrier height about 2.5 kcal/mol lower than the abstraction of a primary hydrogen. Thus, the secondary hydrogen abstraction contributes substantially more than the primary one, although the latter contribution increases with temperature. As to the relative contribution of H_{p1} and H_{p2} to the primary hydrogen abstraction thermal rate, the abstraction of H_{p1} is more

Table 15. μOMT Transmission Coefficients and CUS/μOMT Thermal Rate Constants (in s^{-1}) for H and D Abstraction from the Primary (p1 and p2) and Secondary (s) H(D) Atoms of Propane by CF_3.

T (K)	$\kappa_{H,p1}$	$k_{H,p1}$	$\kappa_{H,p2}$	$k_{H,p2}$	$\kappa_{H,s}$	$k_{H,s}$	$\kappa_{D,p1}$	$k_{D,p1}$	$\kappa_{D,p2}$	$k_{D,p2}$	$\kappa_{D,s}$	$k_{D,s}$
300	2.73	6.25(−20)	2.95	3.59(−20)	2.89	1.82(−18)	3.12	1.69(−20)	3.01	1.04(−20)	1.81	3.83(−19)
400	1.75	3.39(−18)	1.83	1.84(−18)	1.87	4.55(−17)	1.92	1.23(−18)	1.87	7.18(−19)	1.40	1.44(−17)
500	1.43	4.63(−17)	1.47	2.42(−17)	1.51	3.74(−16)	1.52	2.02(−17)	1.50	1.13(−17)	1.24	1.53(−16)
600	1.28	3.02(−16)	1.31	1.53(−16)	1.34	1.70(−15)	1.34	1.50(−16)	1.33	8.16(−17)	1.16	8.25(−16)
700	1.20	1.26(−15)	1.22	6.24(−16)	1.24	5.40(−15)	1.24	6.87(−16)	1.23	3.64(−16)	1.12	3.31(−15)

favorable even when the barrier height and the vibrational adiabatic potential are very similar for the two cases.

The vibrationally adiabatic potentials of reactions R7s, R8s, R7p1, R8p1, R7p2, and R8p2 present two maxima with similar energies, and so CUS calculations are carried out. Some of these reactions also have variational effects. For instance, variational effects are important in reactions R7s and R7p2.

The transmission coefficients are listed in Table 15. The rate constants for reaction R7 are plotted in Figure 14 and tabulated in Table 15 and the Supporting Information. Although the series of reactions studied here was chosen (on the basis of our previous results with an AM1 potential energy surface) to illustrate the new method for efficient calculation of LCT contributions, with the implicit surface of the new direct dynamics calculations, the tunneling contributions to the rate constants are relatively small and well accounted for the SCT approximation. Nevertheless, it is important to have an efficient algorithm for LCT because one does not know a priori which kind of tunneling approximation will be more appropriate, and therefore, it is advisable, when possible and in the absence of experience on similar systems, to carry out both SCT and LCT calculations and to use the μOMT approximation.

Arican et al.[30] also reported the ratio between the abstraction of a secondary and a primary hydrogen. They obtain a ratio k_{R7s}/k_{R7p} of 4.52 and 2.69 at $T = 400$ and 500 K, respectively. The values obtained by CUS/μOMT theory at the same two temperatures are 8.70 and 5.30, respectively. Figure 15 shows that the CUS/μOMT values overestimate the importance of the abstraction of a secondary hydrogen versus the primary hydrogens as compared to the experiment.

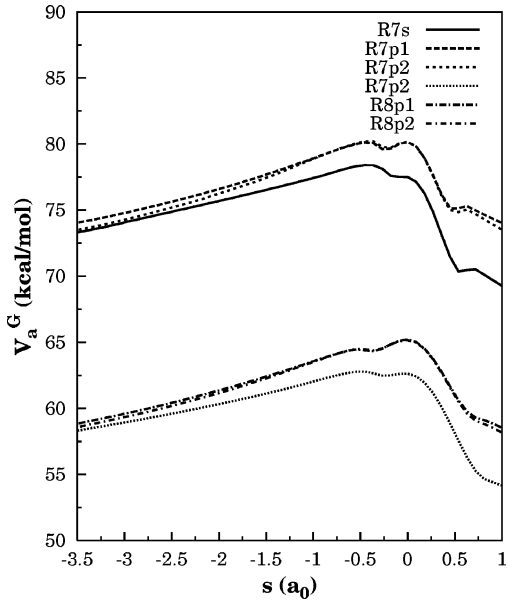

Figure 13. Vibrationally adiabatic potential for reactions R7 and R8.

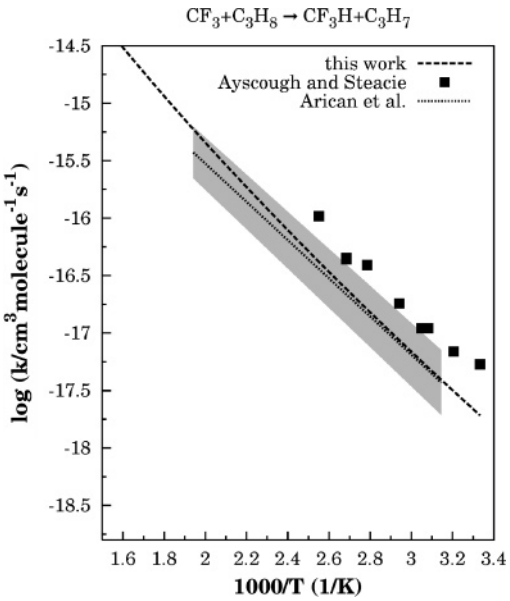

Figure 14. Arrhenius plot for reaction R7. The gray area indicates the standard deviation reported by Arican et al.[30]

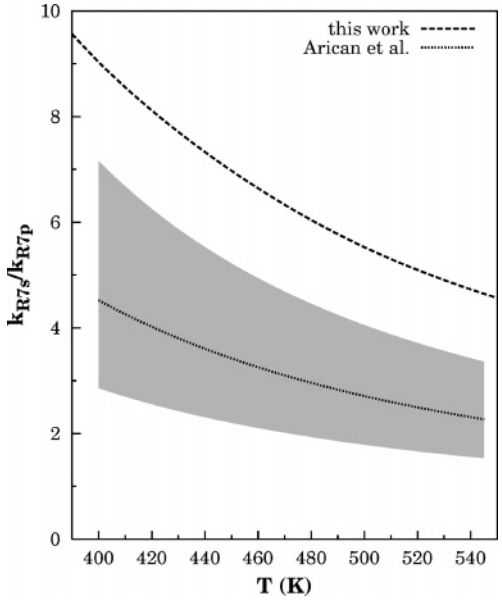

Figure 15. Ratio between the secondary and primary rate constants. The gray area indicates the standard deviation reported by Arican et al.[30]

Table 16. Factors in KIEs for Reactions R7s and R8s[a]

T (K)	η_{tun}	η_{vib}^{TST}	η_{TST}	η_{var}	η^{CUS}	η^{QC}	η
300	1.60	3.35	5.60	0.43	1.24	2.98	4.76
314.9	1.54	3.10	5.18	0.45	1.23	2.87	4.42
367.8	1.40	2.48	4.15	0.51	1.18	2.52	3.52
400	1.34	2.23	3.72	0.54	1.17	2.36	3.16
466.1	1.25	1.87	3.13	0.59	1.15	2.12	2.64
500	1.22	1.74	2.91	0.61	1.14	2.02	2.45
522.9	1.20	1.67	2.78	0.62	1.14	1.96	2.34
600	1.15	1.48	2.46	0.64	1.14	1.79	2.06
626.8	1.14	1.42	2.38	0.64	1.14	1.74	1.98
700	1.11	1.31	2.19	0.59	1.14	1.47	1.63

[a] $\eta_{trans} = 1.16$ and $\eta_{rot}^{TST} = 1.44$.

Table 17. Experimental and Theoretical (CUS/μOMT) Arrhenius Parameters (in cm^3 molecule^{-1} s^{-1} and in kcal/mol) for Reactions R1−R5 and R7 Obtained in the Experimental Range of Temperatures[a,b]

	CUS/μOMT values		experimental values		
reaction	log A	E_a	log A	E_a	T range
R1	−12.0	11.5	−12.1	11.0± 0.5	395−524[c]
			−11.8	11.7	357.3−533.8[d]
R2	−12.4	11.8	−12.7	11.2 ± 0.3	314.9−626.8[e]
R3	−12.1	12.7	−12.0	13.4 ± 0.3	314.9−626.8[e]
R4	−11.8	13.0	−12.6	12.8 ± 2.1	379.4−560[d]
R5	−11.4	9.8	−12.1	8.2 ± 0.5	353.5−489[c]
			−11.9	8.6 ± 0.2	297.6−617[f]
R7	−11.9	8.1	−12.1	7.2 ± 0.5	300−392[g]
			−12.2	7.6 ± 0.2	318−505[h]

[a] CUS/μOMT reduces to CVT/μOMT when there is only one local maximum in the free energy of activation profile and to TST/μOMT when the single maximum occurs at the saddle point. [b] The experimentalists' stated error bar is given when it is more than one in the last digit. [c] Ayscough et al.[27] [d] Carmichael and Johnston.[31] [e] Sharp and Johnston.[29] [f] Arican and Arthur.[32] [g] Ayscough and Steacie.[28] [h] Arican et al.[30]

The KIEs for propane are dominated by the abstraction of secondary hydrogens. The factorization for the secondary abstraction is given in Table 16, which shows that quasiclassical vibrational effects are more important than tunneling and that variational effects lower the KIE by about a factor of 2.

5.4. Arrhenius Parameters. The experimentalists fit their results to an Arrhenius form

$$k = A \exp(-E_a/RT) \tag{28}$$

and for comparison, we made the same kind of fits to the theoretical data. Table 17 shows good agreement in the magnitudes of the Arrhenius parameters for reactions R1−R4; furthermore, theory and experiment agree that the activation energy E_a is considerably smaller for R5 and R7 than for R1−R4, but the preexponential factor A is almost the same. The lowering of the activation energy follows directly from the lower barrier heights in Table 2. It will be interesting to confirm whether MPWB1K gets the substituent effects wrong or whether the discrepancy is due to experimental error.

6. Concluding Remarks

Heavy−light−heavy bimolecular reactions are perhaps the most difficult class of reactions for quantum mechanical calculations of rate constants. We have presented a new, efficient algorithm for LCT calculations, and we illustrate it by straight direct dynamics calculations based on DFT for reactions with five to seven heavy (nonhydrogenic) atoms. This algorithm allowed us to do direct dynamical calculations on a reaction with up to 7 heavy atoms and 15 total atoms (45 degrees of freedom) with quantized generalized normal-mode vibrational frequencies based on curvilinear coordinates, torsional anharmonicity, and optimized multidimensional tunneling. This allowed tests of implicit density functional theory potential energy surfaces against the experiment.

Acknowledgment. The authors are grateful to Ben Ellingson, Steve Mielke, and Yan Zhao for assistance. This work was supported, in part, by the Office of Basic Energy Sciences of the U.S. Department of Energy. A.F. thanks the Ministerio de Educación y Ciencia for a Ramón y Cajal Research Contract and for the Project No. BQU2003-01639.

Supporting Information Available: Tables of theoretical and experimental rate constants, KIEs for abstraction of H from primary and secondary positions in propane, and factors in various KIEs. This material is available free of charge via the Internet at http://pubs.acs.org.

References

(1) Gonzalez-Lafont, A.; Truong, T. N.; Truhlar, D. G. *J. Phys. Chem.* **1991**, *95*, 4618.

(2) Wang, I.; Karplus, M. *J. Am. Chem. Soc*. **1973**, *95*, 8160.

(3) Truhlar, D. G.; Duff, J. W.; Blais, N. C.; Tully, J. C.; Garrett, B. C. *J. Chem. Phys*. **1982**, *77*, 764.

(4) Car, R.; Parrinello, M. *Phys. Rev. Lett*. **1985**, *55*, 2471. Galli, G.; Parrinello, M. *NATO Adv. Sci. Inst. Ser., Ser. E* **1991**, *205*, 283.

(5) *Tight-Binding Approach to Computational Materials Science*; Turchi, P. E. A., Gonis, A., Colombo, L., Eds.; Materials Research Society: Warrendale, PA, 1998.

(6) LeForestier, C. *J. Chem. Phys*. **1978**, *68*, 4406. Helgaker, T.; Uggerud, E.; Jensen, H. J. A. *Chem. Phys. Lett.* **1990**, *173*, 145. Uggerud, E.; Helgaker, T. *J. Am. Chem. Soc*. **1992**, *114*, 4265. Millam, J. M.; Bakken, V., Chem, W.; Hase, W. L.; Schlegel, H. B. *J. Chem. Phys*. **1999**, *111*, 3800. Yu, H.-G.; Muckerman, J. T.; Francisco. J. S. *J. Phys. Chem. A* **2005**, in press.

(7) Truhlar, D. G.; Gordon, M. S. *Science* **1990**, *249*, 491.

(8) Liu, Y.-P.; Lynch, G. C.; Truong, T. N.; Lu, D.-h.; Truhlar, D. G.; Garrett, B. C. *J. Am. Chem. Soc*. **1993**, *115*, 2408.

(9) Liu, Y.-P.; Lu, D.-h.; Gonzàlez-Lafont, A.; Truhlar, D. G.; Garrett, B. C. *J. Am. Chem. Soc*. **1993**, *115*, 7806.

(10) Baldridge, K. K.; Gordon, M. S.; Steckler, R.; Truhlar, D. G. *J. Phys. Chem*. **1989**, *93*, 5107. Truhlar, D. G. *Understanding Chem. React*. **1995**, *16*, 229. Pu, J.; Truhlar, D. G. *J. Chem. Phys*. **2002**, *116*, 1468.

(11) Tuckerman, M. E. *Neumann Inst. Comput. Ser*. **2002**, *10*, 299.

(12) Truhlar, D. G.; Gao, J.; Alhambra, C.; Garcia-Viloca, M.; Corchado, J.; Sanchez, M. L.; Villà, J. *Acc. Chem. Res*. **2002**, *35*, 341. Truhlar, D. G.; Gao, J.; Garcia-Viloca, M.; Alhambra, C.; Corchado, J.; Sanchez, M. L.; Poulsen, T. D. *Int. J. Quantum Chem*. **2004**, *100*, 1136.

(13) Pople, J. A. In *Energy, Structure, and Reactivity*; Smith, D. W., McRae, W. B., Eds.; Wiley: New York, 1973; p 51.

(14) Castillo, J. F.; Aoiz, F. J.; Bañares, L.; Collins, M. A. *J. Phys. Chem. A* **2004**, *108*, 6611. Lin, H.; Pu, J.; Albu, T. V.; Truhlar, D. G. *J. Phys. Chem. A* **2004**, *108*, 4112.

(15) Truhlar, D. G. Kuppermann, A. *J. Chem. Phys*. **1972**, *56*, 2232 and references therein.

(16) Marcus, R. A.; Coltrin, M. E. *J. Chem. Phys*. **1977**, *67*, 2609. Babamov, V. K.; Marcus, R. A. *J. Chem. Phys*. **1978**, *74*, 1790. Garrett, B. C.; Truhlar, D. G. *Proc. Natl. Acad. Sci. U.S.A*. **1979**, *76*, 4755. Skodje, R. T.; Truhlar, D. G.; Garrett, B. C. *J. Chem. Phys*. **1982**, *77*, 5955.

(17) Garrett, B. C.; Truhlar, D. G.; Wagner, A. F.; Dunning, T. H., Jr. *J. Chem. Phys*. **1983**, *78*, 4400. Bondi, D. K.; Connor, J. N. L.; Garrett, B. C.; Truhlar, D. G. *J. Chem. Phys*. **1983**, *78*, 5989.

(18) Garrett, B. C.; Truhlar, D. G. *J. Chem. Phys*. **1983**, *79*, 4931.

(19) Kreevoy, M. M.; Ostovic, D.; Truhlar, D. G.; Garrett, B. C. *J. Chem. Phys*. **1986**, *90*, 3766.

(20) Allison, T. C.; Truhlar, D. G. In *Modern Methods for Multidimensional Dynamics Computations in Chemistry*; Thompson, D. L, Ed.; World Scientific: Singapore, 1998; p 618.

(21) Pu, J.; Truhlar, D. G. *J. Chem. Phys*. **2002**, *117*, 1479.

(22) Garrett, B. C.; Truhlar, D. G. *J. Chem. Phys*. **1980**, *72*, 3460. Garrett, B. C.; Truhlar, D. G.; Grev, R. S.; Magnuson, A. W. *J. Phys. Chem*. **1980**, *84*, 1730, **1983**, *87*, 4554(E).

(23) Truhlar, D. G.; Isaacson, A. D.; Garrett, D. C. In *Theory of Chemical Reaction Dynamics*; Baer, M., Ed.; CRC Press: Boca Raton, FL, 1985; p 65.

(24) Truhlar, D. G.; Brown, F. B.; Steckler, R.; Isaacson, A. D. *NATO Adv. Sci. Inst. Ser., Ser. C* **1986**, *170*, 285.

(25) Lu, D.-h.; Truong, T. N.; Melissas, V. S.; Lynch, G. C.; Liu, Y.-P.; Garrett, B. C.; Steckler, R.; Isaacson, A. D.; Rai, S. N.; Hancock, G. C.; Lauderdale, J. G.; Joseph, T.; Truhlar, D. G. *Comput. Phys. Commun*. **1992**, *71*, 235.

(26) Fernandez-Ramos, A.; Truhlar, D. G. *J. Chem. Phys*. **2001**, *114*, 1491.

(27) Ayscough, P. B.; Polanyi, J. C.; Steacie, E. W. *Can. J. Chem*. **1955**, *33*, 743.

(28) Ayscough, P. B.; Steacie, E. W. R. *Can. J. Chem*. **1956**, *34*, 103.

(29) Sharp, T. E.; Johnston, H. S. *J. Chem. Phys*. **1962**, *37*, 1541.

(30) Arican, H.; Potter, E.; Whytock, D. A. *J. Chem. Soc*., *Faraday Trans*. **1973**, *69*, 1811.

(31) Carmichael, H.; Johnston, H. S. *J. Phys. Chem*. **1964**, *41*, 1975.

(32) Arican, H.; Arthur, N. L. *Int. J. Chem. Kinet*. **1986**, *18*, 437.

(33) Ochterski, J. W.; Petersson, G. A.; Montgomery, J. A. *J. Chem. Phys*. **1996**, *104*, 2598.

(34) Curtiss, L. A.; Redfern, P. C.; Raghavachari, K.; Pople, J. A. *J. Chem. Phys*. **2001**, *114*, 108.

(35) Lynch, B. J.; Truhlar, D. G. *J. Phys. Chem. A* **2003**, *107*, 3898.

(36) Lynch, B. J.; Truhlar, D. G. *ACS Symp. Ser*. **2005**, in press.

(37) Lynch, B. J.; Truhlar, D. G. *J. Phys. Chem. A* **2001**, *105*, 2936.

(38) Zhao, Y.; Lynch, B. J.; Truhlar, D. G. *J. Phys. Chem. A* **2004**, *108*, 2715.

(39) Zhao, Y.; Truhlar, D. G. *J. Phys. Chem. A* **2004** *108*, 6908.

(40) Zhao, Y.; Lynch, B. J.; Truhlar, D. G. *J. Phys. Chem. A* **2004**, *108*, 4786.

(41) Afeefy, H. Y.; Liebman, J. F.; Stein, S. E. *NIST Standard Reference Database* **2003**, *69* (http://webbook.nist.gov).

(42) Zhao, Y.; Lynch, B. J.; Truhlar D. G. *J. Phys. Chem. A* **2004**, *108*, 6908.

(43) Lynch, B. J.; Zhao, Y.; Truhlar, D. G. *J. Phys. Chem. A* **2003**, *107*, 1384.

(44) Hehre, W. J.; Ditchfield, R.; Pople, J. A. *J. Chem. Phys*. **1972**, *56*, 2257.

(45) Hammond, G. S. *J. Am. Chem. Soc*. **1955**, *77*, 334.

(46) Tucker, S. C.; Truhlar, D. G. *NATO Adv. Sci. Inst. Ser., Ser. C* **1989**, *267*, 291.

(47) Jackels, C. F.; Gu, Z.; Truhlar, D. G. *J. Chem. Phys*. **1995**, *102*, 3188.

(48) Chuang, Y.-Y.; Truhlar, D. G. *J. Chem. Phys*. **2000**, *112*, 1221; **2004**, *121*, 7036(E); **2005**, another erratum in preparation.

(49) Pitzer, K. S. *J. Chem. Phys*. **1946**, *14*, 239.

(50) Fernandez-Ramos, A.; Truhlar, D. G. *J. Phys. Chem*. **2002**, *106*, 4957.

(51) Corchado, J. C.; Chuang, Y.-Y.; Fast, P. L.; Villà, J.; Hu, W.-P.; Liu, Y.-P.; Lynch, G. C.; Nguyen, K. A.; Jackels, C. F.; Elllingson, B.; Melissas, V. S.; Lynch, B. J.; Rossi, I.; Coitiño, E. L.; Fernandez-Ramos, A.; Pu, J.; Albu, T. V.; Steckler, R.; Garrett, B. C.; Isaacson, A. D.; Truhlar, D. G. *POLYRATE*, version 9.3.1; University of Minnesota: Minneapolis, MN, 2005.

(52) Corchado, J. C.; Chuang, Y.-Y.; Coitiño, E. L.; Truhlar, D. G. *GAUSSRATE*, version 9.1; University of Minnesota: Minnespolis, MN, 2003.

(53) Frisch, M. J.; Trucks, G. W.; Schlegel, H. B.; Scuseria, G. E.; Robb, M. A.; Cheeseman, J. R.; Montgomery, Jr., J. A.; Vreven, T.; Kudin, K. N.; Burant, J. C.; Millam, J. M.; Iyengar, S. S.; Tomasi, J.; Barone, V.; Mennucci, B.; Cossi, M.; Scalmani, G.; Rega, N.; Petersson, G. A.; Nakatsuji, H.; Hada, M.; Ehara, M.; Toyota, K.; Fukuda, R.; Hasegawa, J.; Ishida, M.; Nakajima, T.; Honda, Y.; Kitao, O.; Nakai, H.; Klene, M.; Li, X.; Knox, J. E.; Hratchian, H. P.; Cross, J. B.; Bakken, V.; Amado, C.; Jaramillo, J.; Gomperts, R.; Stratmann, R. E.; Yazyev, O.; Austin, A. J.; Cammi, R.; Pomelli, C.; Ochterski, J. W.; Ayala, P. Y.; Morokuma, K.; Voth, G. A.; Salvador, P.; Dannenberg, J. J.; Zakrzewski, V. G.; Dapprich, S.; Daniels, A. D.; Strain, M. C.; Farkas, O.; Malick, D. K.; Rabuck, A. D.; Raghavachari, K.; Foresman, J. B.; Ortiz, J. V.; Cui, Q.; Baboul, A. G.; Clifford, S.; Cioslowski, J.; Stefanov, B. B.; Liu, G.; Liashenko, A.; Piskorz, P.; Komaromi, I.; Martin, R. L.; Fox, D. J.; Keith, T.; Al-Laham, M. A.; Peng, C. Y.; Nanyakkara, A.; Challacombe, M.; Gill, P. M. W.; Johnson, B.; Chen, W.; Wong, M. W.; Gonzalez, C.; Pople, J. A.; *Gaussian 03*, revision C.02; Gaussian, Inc.: Wallingford, CT, 2004.

(54) Page, M.; McIver, J. W., Jr. *J. Chem. Phys*. **1988**, *88*, 922.

(55) Chuang, Y.-Y.; Truhlar, D. G. *J. Phys. Chem. A* **1998**, *102*, 242.

(56) Garrett, B. C.; Truhlar, D. G. *J. Phys. Chem*. **1979**, *83*, 2921.

(57) Dybala-Defratyka, A.; Paneth, P.; Pu, J.; Truhlar, D. G. *J. Phys. Chem. A* **2004**, *108*, 2475.

(58) Hu, W.-P.; Truhlar, D. G. *J. Am. Chem. Soc*. **1995**, *117*, 10726.

CT050153I